Solar Energy 155 (2017) 847–853

Contents lists available at ScienceDirect

Solar Energy

journal homepage: www.elsevier.com/locate/solener

# Progress in the explanation and modeling of the laser-induced damage of edge-isolation processes in crystalline silicon solar cells

Alona Otaegi *, Vanesa Fano, Muhammad Azam Rasool, José Rubén Gutiérrez, Juan Carlos Jimeno, Nekane Azkona, Eneko Cereceda

*Technological Institute for Microelectronics, University of the Basque Country, 48013 Bilbao, Spain*

ARTICLE INFO

*Article history:*
Received 30 January 2017
Received in revised form 27 June 2017
Accepted 7 July 2017
Available online 26 July 2017

*Keywords:*
Solar cells
Laser-induced damage
Ideality factor
Modeling

ABSTRACT

Laser processes in solar cells are the origin of a considerable mechanical and electrical damage. This paper introduces a model that presents a good fitting to the laser-induced damage, previously characterized as an extra recombination diode, with a highly variable ideality factor, connected to the rest of the structure through an interconnecting resistance, determined by the geometry of the damage and the sheet resistance of the interconnecting layers. In this work, the interconnecting resistance appears to be several orders of magnitude over the expected geometrical value and dependent on the nature of the laser used; the extra recombination diode originated by the laser-induced damage has been found of lower dependence from the laser parameters used and, in all the cases, with an ideality factor of 2. The effect of the laser-induced damage on the *I-V* curve of the solar cells and the reduction of their $V_{OC}$ appears to be mainly dependent on the value of this interconnecting resistance which connects or disconnects the damage from the rest of the cell. A soft chemical treatment, compatible with the passivating $SiN_x$ layer, increases the value of this resistance in more than one order of magnitude.



## 1. Introduction

Laser processes in solar cells are the origin of mechanical and electrical damage well known in literature (Cereceda et al., 2012; Grohe et al., 2006; Otaegi et al., 2010; Abbott et al., 2005; Sugianto et al., 2010). Apart from the evident mechanical damages associated to the laser process and their mitigation (Cereceda et al., 2012), the laser-induced damage has two mayor consequences, already analyzed in previous literature: (a) the dark *I–V* curve is modified due to the appearance of a hump in the voltage range of 200–400 mV (Grohe et al., 2006; Otaegi et al., 2010) and (b) a decrease on the open-circuit voltage (Abbott et al., 2005; Sugianto et al., 2010). The hump behavior is modeled by an extra recombination diode connected to the non-damaged cell through an interconnecting resistance (Hernando et al., 1998). This model is used in the characterization of laser-induced damage, in the case of laser isolation (McIntosh and Honsberg, 2001; Gutscher et al., 2008; Otaegi et al., 2012) and in the case of laser doping (Sugianto et al., 2007). The interconnecting resistance has been analyzed to be only dependent on the geometry of the structure and the resistivity of the emitter, with values in a range of 1–10 Ω cm (McIntosh and Honsberg, 2001; Gutscher et al., 2008; Sugianto et al., 2007; Tjahjono et al., 2007), therefore, independent from the damage introduced; the characterization of the laser-induced damage has been then relegated to analyze the role of the additional recombination diode. A very variable ideality factor, with values in the range of 2–6 (Gutscher et al., 2008; Sugianto et al., 2007; Tjahjono et al., 2007; Breitenstein et al., 2006; Steingrube et al., 2010), has been assigned to this extra diode; however, the well-known Shockley-Read-Hall, SRH, recombination model stands that the ideality factor cannot exceed values larger than 2 (Ashburn et al., 1975; McIntosh et al., 2001). Recently, complex mechanisms have been found to explain these high ideality values of the ideality factor that can appear in highly damaged regions (Breitenstein et al., 2006; Steingrube et al., 2010).

This works shows two cases of laser-induced damage in an equivalent process to the edge isolation of solar cells. The damage is recovered in some of the samples with alkaline etching (Abbott et al., 2005). Results have shown the appearance of a hump with an ideality factor from 2 to 6, according to previous works, but this hump can be modeled by an additional recombination diode with an ideality factor of 2, according to the conventional SRH recombination model; the resistance that connects the damage with the rest of the solar cell is even several orders of magnitude over the expected geometrical value and dependent on the nature of

* Corresponding author.
*E-mail address:* alona.otaegi@ehu.eus (A. Otaegi).

http://dx.doi.org/10.1016/j.solener.2017.07.030
0038-092X/

the laser used and the recovery process. The understanding of the damage nature helps to validate the laser processes for the manufacturing of high efficiency solar cells, opening this technology to edge isolation, back-contact formation or any other manufacturing step.

## 2. Characterization of the laser-induced damage

The analysis of the laser-scribing of solar cells on their front emitter had shown the degradation of their $I_{SC}$-$V_{OC}$ characteristics (Otaegi et al., 2012, 2015). Starting from industrial solar cells, lines of different lengths have been laser-scribed in their front side using two different laser wavelengths, the infrared, IR, 1030 nm and the green, GR, 515 nm. A couple of pulse energies of the pulsed-laser have been used in the GR case and only one in the IR case but always using laser parameters close to those needed for the edge isolation process, giving to grow depths in the 15–25 μm range. Fig. 1 shows the results of these experiments with the apparition of a hump, an extra recombination current in the 200–400 mV range, with an apparent ideality factor from 4 to 6.

To model this damage, the conventional electrical circuit, shown in Fig. 2, for the hump (Hernando et al., 1998) and the laser-induced damage (McIntosh and Honsberg, 2001) has been used. In this circuit, an extra recombination diode with current $J_h$ is added to the conventional double diode model of the solar cell. This extra diode is connected to the solar cell by means of an interconnecting resistance, $R_h$. From the analysis of the data from Fig. 1 it has been shown that the value of the inverse of this interconnecting resistance grows linearly with the length of the damaged line, as expected, but it is not related to the geometrical value, as it is assumed in other works (McIntosh and Honsberg, 2001; Gutscher et al., 2008; Sugianto et al., 2007; Tjahjono et al., 2007), being even an order of magnitude over this geometrical value. The laser-induced damage only has affected to the $J_h$ or $R_h$ parameters but not to the rest of parameters from the conventional solar cell. At this point, not reliable information has been obtained about the characteristics of the extra diode $J_h$.

## 3. Assessment of the surface damage induced by the laser

In order to obtain the internal parameters of the hump recombination diode, through its saturation current, $J_{0h}$, and the ideality factor, $m_h$, two batches of solar cells have been processed, which include a large ratio of laser-scribed perimeter to cell area. That is done according to the cell geometry shown in Fig. 3, corresponding to a laser-scribed perimeter of 71.4 cm for a 13.4 $cm^2$ cell area.

The laser-system used to perform the experiments consists of a Q-switched fiber laser, which generates pulses of 10 ns duration, a Gaussian beam with a circular spot of 30 μm diameter, working at two wavelengths (infrared, IR, $\lambda_1$ = 1030 nm and green, GR, $\lambda_2$ = 515 nm). A high speed x-y galvano-mechanical beam positioner allows scanning samples in a 160 mm × 160 mm platform. Table 1 shows the laser parameters used for the laser-scribing process, conditions that are equivalents for an edge laser-isolation process with laser-grooves from 15 to 25 μm depth for the laser used.

The process used to manufacture the solar cells is shown in Fig. 4. Batch A and batch B solar cells were processed starting from 0.5 to 2 Ω cm *p*-type monocrystalline Cz-silicon wafers, and solar cells were fabricated with a 50–60 Ω/□ $POCl_3$ diffused emitter. The front-side AR coating consisted of a silicon nitride layer deposited by PECVD on a random pyramid textured surface. A screen printed aluminum BSF structure was used in the rear side. Front and rear contacts were screen printed and co-fired in an infrared belt furnace, aluminum and silver aluminum pastes on the rear side and a silver paste on the front side.

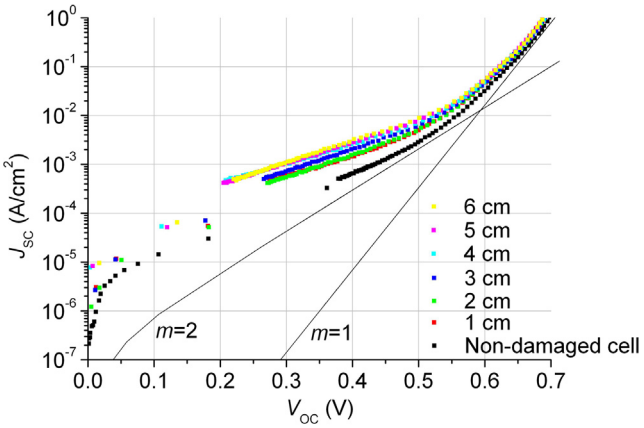


**Fig. 1.** $J_{SC}$-$V_{OC}$ characteristics for different IR laser-scribing lengths.

The difference between batch A and batch B was the order an additional step of alkaline chemical treatment was carried out. Alkaline etches are conventional processes in the recovery of laser-damaged cells (Abbott et al., 2005; Du et al., 2012) and focused on analyzing how this recovery affects to the damaged cell, solar cells were chemically treated by a 25 wt% NaOH solution at 60 °C; the silicon estimated etching-rate at these conditions is ~0.2 μm/min. and the $SiN_x$ layer resists to this etching for times until 5 min. The etching was applied for times from 3 to 5 min, the shorter times in batch A because the target was only to verify if this etching affects to the final characteristics without compromising the integrity of the $SiN_x$ layers. Table 2 shows the characteristics of the four processes made.

## 4. Results and discussion

Solar cells have been characterized by measuring illumination and dark *I–V* curves. Fittings of the curves have been made with the MultIV program (Martínez, 1992).

Fig. 5 shows the illumination and dark *I-V* characteristics for two solar cells, from batch A and batch B, laser-scribed by the IR laser. The square and circle dots correspond to the *I-V* curves under illumination and the triangular and rhombus dots correspond to the dark *I-V* curves representation, red[1] color to distinguish the batch A solar cells from the batch B processed solar cells represented in blue.

The analysis of the *I-V* curves under illumination has shown an extra contribution of the short-circuit current for batch A processed solar cells due to the poor isolation of their internal laser-scribed rectangles compared to batch B solar cells. The reduction in current for batch B corresponded to this area effectively isolated by the laser, as the decrease consisted of a 12.5%. Due to the damage recovery, from the chemical treatment introduced, batch B solar cells, GR or IR laser-scribed, have shown an increment on the $V_{OC}$ between 10 and 50 mV regarding their equivalents from batch A, which denotes a reduction on the laser-induced damage. These data are summarized in Table 3.

Regarding the dark *I-V* curves, for batch A processed solar cells the fitting to a conventional double diode model has presented fitting errors under 5%, what is coherent with the error from the measured data. For this batch A processed solar cells, the second exponential current, ranging from $3{\cdot}10^{-7}$ to $9{\cdot}10^{-7}$ A/$cm^2$, has

[1] For interpretation of color in Figs. 5 and 6, the reader is referred to the web version of this article.

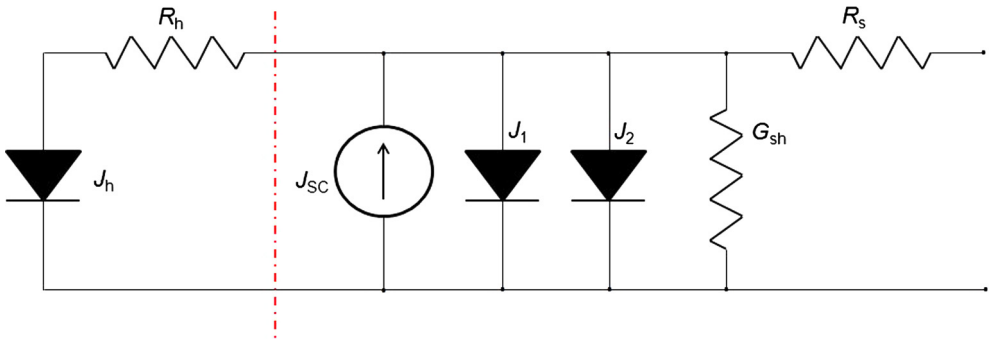


**Fig. 2.** Equivalent circuit representation of a standard solar cell with a resistively isolated region.

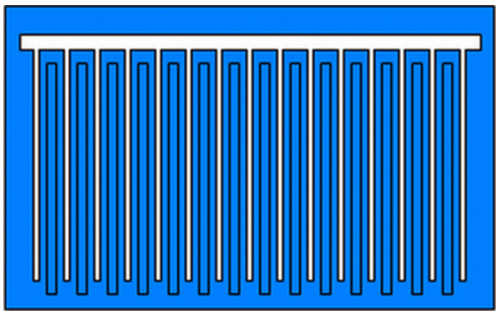

**Fig. 3.** Solar cell with 14 rectangles laser-scribed between metallic fingers.

**Table 1**
Laser parameters for the batch-processing.

| Laser | Velocity | *PRF* | $E_{pulse}$ | Scribing-times |
|---|---|---|---|---|
| GR | 500 mm/s | 50 kHz | 240 μJ | 8 times |
| IR | 500 mm/s | 50 kHz | 480 μJ | 4 times |

masked completely the first exponential current. For batch B processed solar cells, however, two performances have been observed: in the case of IR laser-scribed solar cells a hump has been observed in the 200–400 mV voltage range, as appears in Fig. 4, while in the GR laser-scribed solar cells the fitting error under the double diode model remained under 5%, and from a first glance, there was no evidence of the existence of a hump.

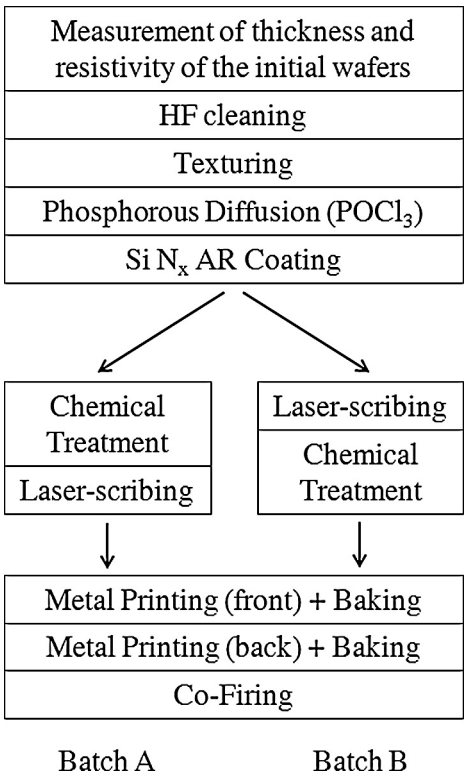


**Fig. 4.** (a) Batch A: laser-scribed and chemically treated solar cells, and (b) Batch B: chemically treated and laser-scribed solar cells; processing steps.

## 5. Modeling the damage

In order to obtain the information from the parameters of the hump diode the dark *I-V* curves of the solar cells have been measured at 15, 25, 35 and 50 °C. Fig. 6 shows the evolution and fittings of the *I-V* curve for the IR laser batch B processed solar cells at 25 and 50 °C. The circular dots in red color represent the dark *I-V* performance of the cell at 25 °C and the red curve represents the fitting to the double diode model. The square dots in blue color represent the dark *I-V* performance of the cell at 50 °C whilst the blue curve represents the fitting. It can be observed that the hump loses importance as the temperature grows: this hump is masked due to the temperature-dependence of the $J_{02}$ current density component. Consequently, the hump is very clearly present at 25 °C, but only slightly noticeable at 50 °C.

The fitting of the *I-V* curves was made first excluding the data in the 100–500 mV voltage range and fitting the rest data to a conventional double exponential model with ideality factors of 1 and 2. The hump contribution was then obtained subtracting the current data in the 100–500 mV voltage range minus the modeled values using the conventional double diode model and the data previously obtained. Fig. 7 shows this contribution in the case of only subtracting the modeled values from the first exponential diode and the shunt conductance. It can be observed that for the low current regime and for the high current regime the performance of the current corresponds to ideality factors of 2; in the high current regime this performance can be modeled by a $J_{02}$ from the classic double diode model and in the low current regime, this behavior can be modeled by a hump, with its $J_{0h}$, and an interconnecting resistance, $R_h$, that makes the transition between the low and the high current regimes.

The fitting of the hump was revealed very complex if the laser-induced damage was very low or very high. For the first case, the contribution of the hump current was obviously masked due to its low value, but in the second case, the hump was high and it was difficult to discern from the conventional second exponential diode. The values of the hump and the second exponential diode presented a correlated behavior and any error in the saturation

**Table 2**
Summary of processing specifications.

| Process | Laser | Description |
|---|---|---|
| Batch A | IR | NaOH + Laser |
| Batch A | GR | NaOH + Laser |
| Batch B | IR | Laser + NaOH |
| Batch B | GR | Laser + NaOH |

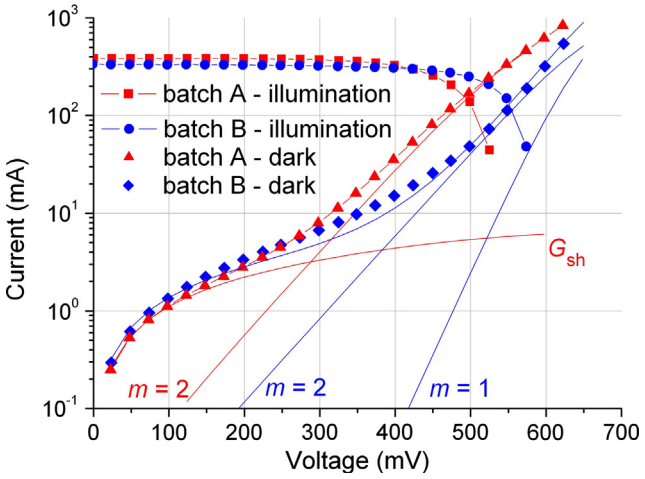


**Fig. 5.** Experimental *I-V* curves under illumination and dark for batch A and batch B processed and IR laser-scribed solar cells.

**Table 3**
Fitting parameters of batch A and batch B solar cells.

| | | Batch A | | Batch B | |
|---|---|---|---|---|---|
| | Reference cell | IR laser | GR laser | IR laser | GR laser |
| $V_{OC}$ (mV) | 597 | 537 | 570 | 583 | 579 |
| $J_{SC}$ (mA/cm$^2$) | 31.6 | 29.9 | 31.0 | 25.1 | 25.1 |

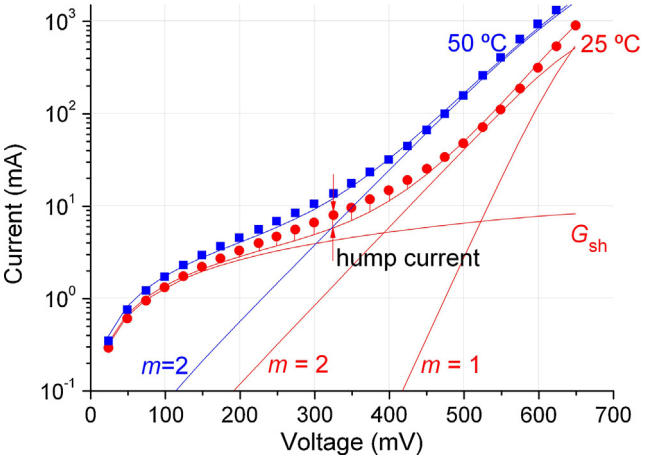


**Fig. 6.** Dark *I-V* current characteristic of an IR laser-damaged cell showing a hump in the 25 °C case but not in the 50 °C case.

current of the second exponential diode caused high variations in the opposite way to the saturation current of the hump. These errors, affect also to the interconnecting resistance, $R_h$; an overestimation of the $J_{02}$ value causes the obtaining of lower hump saturation currents, $J_{0h}$, and an increase in the $R_h$ value. The activation energies obtained suffer from similar behavior: an overestimation

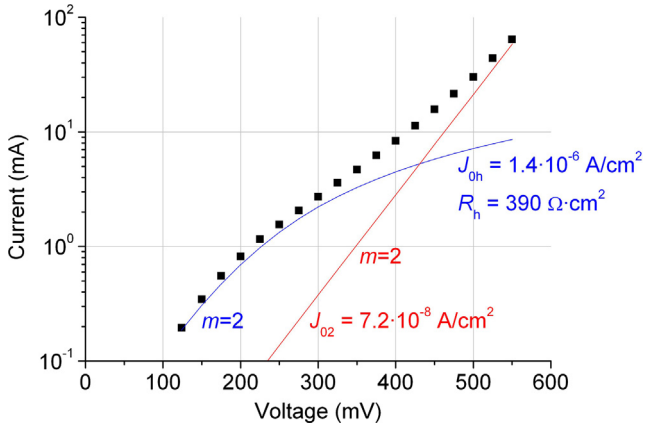


**Fig. 7.** Dark *I-V* characteristics of a laser-damaged solar cell after deducting the contributions of the shunt conductance and the first exponential diode.

of the activation energy of the second exponential diode of the solar cell causes the obtaining of lower activation energies of the hump and negative activation energies for the interconnecting resistance. Table 4 shows the best fittings obtained according to the previously explained procedure. The activation energies of the first exponential diode have been obtained to be 1.2 eV, which is usually associated to recombination into the base area. Fig. 8 shows the activation energy of the second exponential diodes, which were sited around 0.5 eV, lower than the expected 0.6 eV, and this activation energy has been obtained to be similar for the humps in batch A as can be observed in Fig. 9. In these cases, the values obtained of the interconnecting resistances remains independent from temperature.

Table 4 includes the fitting parameters of a reference cell manufactured with the same process presented in Fig. 4 but avoiding the chemical treatment and the laser-scribing steps. For the analyzed cells, the values of the first exponential diode remain independent from the process, in a range of 6·10$^{-13}$–1.1·10$^{-12}$ A/cm$^2$ and are equivalent to the reference cell. For cells from the batch A, the values of the second exponential diode range from 3·10$^{-7}$ to 6·10$^{-7}$ mA/cm$^2$, being higher for the IR laser processed cells than for the GR laser processed cells; however, for the batch B, this second exponential diode recovers down to values close to the reference cell, from 4·10$^{-8}$ to 6·10$^{-8}$ A/cm$^2$, with values slightly higher for the IR laser processed cells. Regarding to the recombination from the second exponential diodes in the low current regime, which is proportional to the $J_{02}$ and $J_{0h}$ addition, it seems low dependent on the application or not of the chemical treatment and more dependent on the initial damage generated from the laser-scribing process, with values ranging from 4.6·10$^{-7}$ to 1.6·10$^{-6}$ A/cm$^2$ with the exception of the GR case of batch B, in which the hump current is complex to have reliable results due to its low value. The transition from the low to the high current regime between the second exponential diodes is determined by the interconnecting resistance $R_h$, as it was indicated in Fig. 7. The interconnecting resistance appears to be dependent on the induced damage, with larger damage for the IR laser, and in all cases, its value increases if the chemical treatment is applied, from 10 to 390 Ω cm$^2$ for the IR laser and from 130 to 1240 Ω·cm$^2$ for the GR laser. It has to be pointed out that for values of $R_h$ over 300 Ω cm$^2$ the influence of the hump on the total current is very small and not reliable parameters would be obtained.

Although the provided parameters of the hump contribution diode, $J_{0h}$ and $R_h$, have been normalized regarding the cell area, obviously the damage should be proportional to the perimeter scribed. Table 5 shows the normalized values for the hump diodes,

**Table 4**
Fitted parameters for the batch A and batch B processed solar cells.

| Reference cell Patrón | Value | Std. dev. | | |
|---|---|---|---|---|
| $J_{01}$ (A/cm$^2$) | $6.04{\cdot}10^{-13}$ | $2.69{\cdot}10^{-13}$ | | |
| $J_{02}$ (A/cm$^2$) | $5.76{\cdot}10^{-8}$ | $1.18{\cdot}10^{-8}$ | | |
| $G_{sh}$ ($\Omega^{-1}$ cm$^{-2}$) | $8.52{\cdot}10^{-3}$ | $1.08{\cdot}10^{-4}$ | | |
| $R_s$ ($\Omega$ cm$^2$) | 1.01 | 0.32 | | |
| **Batch A – IR laser** | **Value** | **Std. dev.** | ***n*** | ***E*$_a$** |
| $J_{01}$ (A/cm$^2$) | – | – | – | – |
| $J_{02}$ (A/cm$^2$) | $6{\cdot}10^{-7}$ | $3{\cdot}10^{-8}$ | 1.5 | 0.52 |
| $G_{sh}$ ($\Omega^{-1}$ cm$^{-2}$) | $7.8{\cdot}10^{-4}$ | $2.8{\cdot}10^{-5}$ | – | – |
| $R_s$ ($\Omega$ cm$^2$) | 0.53 | 0.08 | – | – |
| $J_{0h}$ (A/cm$^2$) | $4.8{\cdot}10^{-7}$ | $3.7{\cdot}10^{-8}$ | 1.5 | 0.52 |
| $R_h$ ($\Omega$ cm$^2$) | 10.7 | 3.1 | – | – |
| **Batch A – GR laser** | **Value** | **Std. dev.** | ***n*** | ***E*$_a$** |
| $J_{01}$ (A/cm$^2$) | – | | | |
| $J_{02}$ (A/cm$^2$) | $3{\cdot}10^{-7}$ | $1.4{\cdot}10^{-8}$ | 1.5 | 0.52 |
| $G_{sh}$ ($\Omega^{-1}$ cm$^{-2}$) | $1.8{\cdot}10^{-4}$ | $6.4{\cdot}10^{-5}$ | – | – |
| $R_s$ ($\Omega$ cm$^2$) | 0.68 | 0.08 | – | – |
| $J_{0h}$ (A/cm$^2$) | $1.6{\cdot}10^{-7}$ | $1.6{\cdot}10^{-8}$ | 1.5 | 0.48 |
| $R_h$ ($\Omega$ cm$^2$) | 130 | 39 | – | – |
| **Batch B – IR laser** | **Value** | **Std. dev.** | ***n*** | ***E*$_a$** |
| $J_{01}$ (A/cm$^2$) | $6.5{\cdot}10^{-13}$ | $2.8{\cdot}10^{-13}$ | 3 | 1.27 |
| $J_{02}$ (A/cm$^2$) | $1.6{\cdot}10^{-7}$ | $2.1{\cdot}10^{-8}$ | 1.5 | 0.52 |
| $G_{sh}$ ($\Omega^{-1}$ cm$^{-2}$) | $9.2{\cdot}10^{-4}$ | $3.2{\cdot}10^{-5}$ | – | – |
| $R_s$ ($\Omega$ cm$^2$) | 0.26 | 0.13 | – | – |
| $J_{0h}$ (A/cm$^2$) | $1.4{\cdot}10^{-6}$ | $2.4{\cdot}10^{-7}$ | 0 | 0 |
| $R_h$ ($\Omega$ cm$^2$) | 390 | 47 | – | – |
| **Batch B – GR laser** | **Value** | **Std. dev.** | ***n*** | ***E*$_a$** |
| $J_{01}$ (A/cm$^2$) | $1.1{\cdot}10^{-12}$ | $8.3{\cdot}10^{-14}$ | 3 | 1.27 |
| $J_{02}$ (A/cm$^2$) | $4.4{\cdot}10^{-8}$ | $2.5{\cdot}10^{-9}$ | 1.5 | 0.5 |
| $G_{sh}$ ($\Omega^{-1}$ cm$^{-2}$) | $5.9{\cdot}10^{-4}$ | $8.4{\cdot}10^{-6}$ | – | – |
| $R_s$ ($\Omega$ cm$^2$) | 0.34 | 0.05 | – | – |
| $J_{0h}$ (A/cm$^2$) | $1{\cdot}10^{-7}$ | $4.8{\cdot}10^{-8}$ | – | – |
| $R_h$ ($\Omega$ cm$^2$) | 1240 | 1200 | – | – |

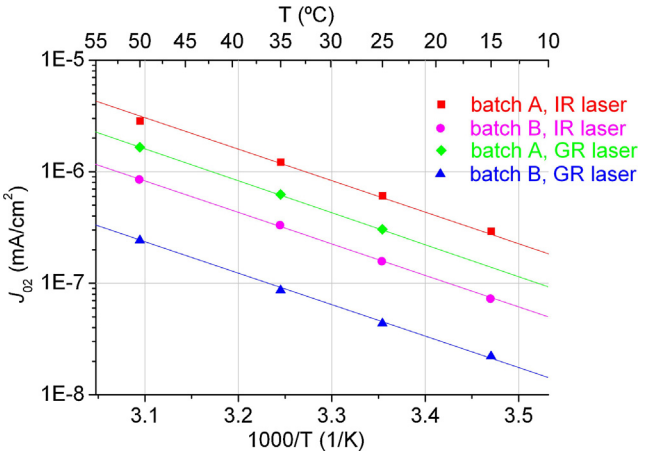


**Fig. 8.** Temperature dependence of the saturation currents of the second exponential diodes.

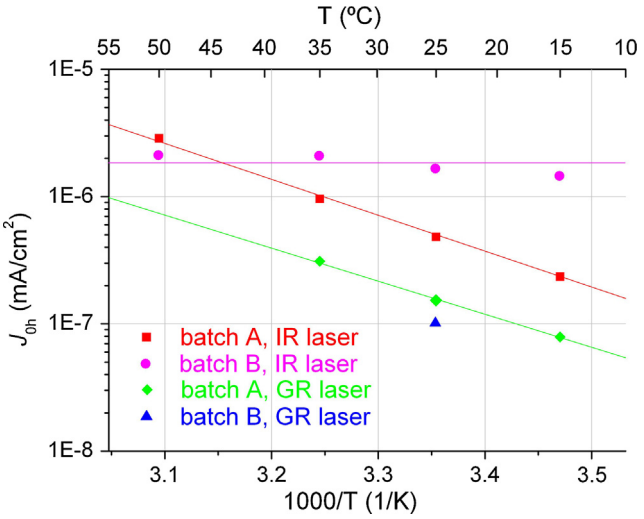


**Fig. 9.** Temperature dependence of the hump saturation currents.

the conventional second exponential diodes and the addition of both $m = 2$ terms, what gives a clear idea of the current transition presented in Fig. 7.

It can be observed that the hump recombination current, proportional to the $\bar{J}_{02} + \bar{J}_{0h}$, presents a narrow range of values, from 90 to 300 nA/cm, except for the case of batch B and GR laser, where the huge value of the $\bar{R}_h$ parameter inhibit the obtaining of a reliable value of the $\bar{J}_{0h}$ saturation current. The analytical calculation of the maximum recombination in a *p-n* junction has been obtained considering the SRH theory. For the depleted region, from $-x_n$ to $x_p$, of a *p-n* junction bordered perpendicularly by a surface with recombination velocity, *S*, the maximum recombination can be approximated by:

$$\bar{J}_h(\mathrm{A/cm}) = 2q\int_{-x_n}^{x_p}\left(s\frac{np-n_i^2}{n+p}\right)dx \approx \frac{qn_iV_T\pi S}{\varepsilon_j}\left(\exp\frac{V}{2V_T}-1\right) \qquad (1)$$

**Table 5**
Quantification of the $\bar{J}_{0h}$ and the $\bar{R}_h$ induced by the lasers.

| | Batch A | | Batch B | |
|---|---|---|---|---|
| | IR laser | GR laser | IR laser | GR laser |
| $\bar{R}_h$ (Ω cm) | 57 | 700 | 2100 | 6600 |
| $\bar{J}_{0h}$ (nA/cm) | 90 | 30 | 264 | 19 |
| $\bar{J}_{02}$ (nA/cm) | 113 | 56 | 30 | 8 |
| $\bar{J}_{0h} + \bar{J}_{02}$ (nA/cm) | 203 | 87 | 294 | 27 |

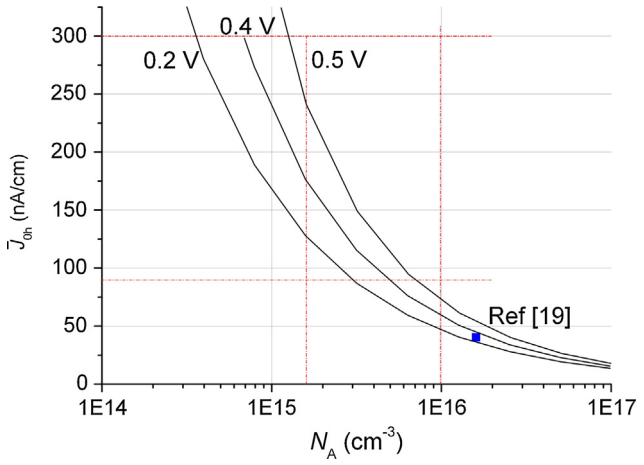


**Fig. 10.** Saturation current of the recombination on a *p-n* junction bordering a surface, as a function of the base doping concentration and $S = 10^7$ cm/s, for three different values of the applied voltage.

being $\varepsilon_j$ the electric field value in the maximum recombination point, where $n = p$. This electric field depends on the doping of the base, $N_A$, and slightly on the applied voltage to the *p-n* junction. The multiplier of 2 is because for every laser-groove, there are two parallel lines of the *p-n* junction bordering the surface. From (1) we can obtain the saturation current of the maximum recombination in the *p-n* junction as:

$$\bar{J}_{0h} = \frac{q n_i V_T \pi S}{\varepsilon_j} \tag{2}$$

Fig. 10 shows the obtained value of this saturation current as a function of the base doping and for three values of applied voltage to the *p-n* junction that modifies slightly this saturation current value. The figure includes also the value of this saturation current obtained by numerical modeling (Kühn et al., 2000). It can be observed that the obtained $\bar{J}_{02} + \bar{J}_{0h}$ values, in the area highlighted between dashed lines, are coherent with the results in Fig. 10.

Finally, the saturation current of the second exponential diode is reduced dramatically in batch B cells, as it is shown in Table 4. Probably this value would correspond to the recombination on the cell area out from the damaged region.

As an interpretation of the results, we believe that, on the one hand, the $\bar{J}_{0h}$ parameter could correspond to the perimeter of a *p-n* junction with high surface recombination velocity and, on the other hand, the $\bar{R}_h$, which increases its value by one order of magnitude depending on the process, could be related to the debris found in the grooves. Fig. 11 shows SEM images for grooves scribed by the GR laser; the debris is easily observed for the batch A processed solar cell, however, no debris is appreciated in batch B after the chemical treatment. This chemical treatment has low effect on the recombination diode, nevertheless, we suspect that a passivation step would diminish its $\bar{J}_{0h}$ value as outlined in Altermatt et al. (1996), Guo et al., (2007), Kyeong et al. (2009).

## 6. Conclusions

Two different laser radiations, IR 1030 nm and GR 515 nm, have been used for scribing the front side of solar cells made by a conventional phosphorus-aluminum technology. The IR radiation produced the greater damage in terms of a considerable reduction, around 50 mV, over the expected $V_{OC}$ value from non-damaged cells. From the analysis of dark *I-V* characteristics a large recombination current dominating the characteristic for the IR case has been obtained. This recombination current exhibited an ideality factor of value 2. For the GR case the dark *I-V* characteristics have shown a hump in the region of 200–400 mV, with very variable ideality factor, being temperature dependent and reaching values from 4 to 6. Other batch of solar cells has been produced with the same process but, in this batch, after the laser-scribing a soft alkaline chemical treatment has been placed in order to recover the cell from the laser-induced damage. In these cases the $V_{OC}$ values recover close to the non damaged cell values and apparently the dark *I-V* characteristics do not present humps. In all the cases the IR damaged cells exhibit poorer characteristics than the GR damaged cells.

A standard hump model has been assumed in which an extra recombination diode is added to the equivalent circuit of the solar cell by means of an interconnecting resistance. In conventional hump modeling, this diode has had an unknown ideality factor,

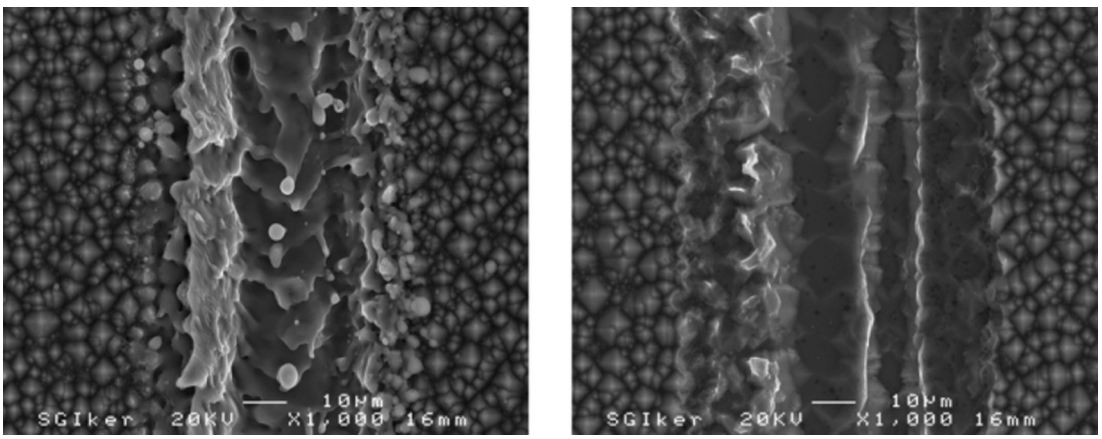


**Fig. 11.** SEM images of the GR laser-scribed grooves: (a) batch A processed solar cell; (b) batch B processed solar cell.

usually greater than 2, and the value of the interconnecting resistance has been determined by the geometry of the cell, the sheet resistance of the different layers and the position of the damaged region. The obtaining of the parameters from these extra components, the saturation current, the ideality factor and the interconnecting resistance, was very sensitive to the fitting procedure of the dark *I-V* characteristics. The use of a special fitting methodology has revealed the apparition of two second exponential diodes with ideality factors equal to 2 but with two different values of saturation currents, being the larger on the low current regime and the smaller in the high current regime. This current behavior had an adequate correspondence with the assumed hump model in which the smaller saturation current corresponded to the conventional second exponential diode of the double diode model and the higher saturation current, obtained at the lower voltages, corresponded to the addition of this second exponential diode's saturation current and the saturation current of the extra recombination diode added to the model. The transition between both saturation currents had been adequately modeled by the interconnecting resistance included in the model.

From the temperature analysis of the characteristics, an activation energy of 0.48–0.52 eV had been obtained for both components of $m = 2$, $J_{02}$ and $J_{0h}$. The interconnecting resistance had values not temperature dependent. However, for the larger $R_h$ values, over 300 Ω cm$^2$, the disconnection of the damage from the rest of the structure was large and their current contribution was usually masked by other current components like the shunt conductance, and the obtaining of reliable values of its components and activation energies was a tricky task. The saturation current of the recombination in the low voltage regime, $J_{02} + J_{0h}$, presented values in a narrow range, with values, once being normalized regarding the length of the laser-induced damage, from 90 to 300 nA/cm that could be explained by a conventional SRH recombination. After the chemical alkaline treatment over the laser-scribing, the saturation current of the conventional second exponential diode was reduced significantly down to values in the 40–160 nA/cm range, what would correspond, in its majority, to recombination in the non-damaged areas. At the same time, the interconnecting resistance increased its value by one order of magnitude reaching values in the 2–6 kΩ cm range. Finally, it can be concluded that the main parameter controlling the influence of the damage in these laser-scribing processes was the interconnecting resistance, more than the recombination diode induced in the damaged region. This recombination diode appeared to have similar values for the different cases analyzed and, in all those cases, with ideality factor of 2 and activation energies of 0.5 eV. However, the interconnecting resistance appeared to have more variable values, regarding the laser used and their effect on the *I-V* characteristic, and these values could be increased in one order of magnitude by the use of a soft alkaline chemical treatment, which respects all previous technological steps including the passivating SiNx layer.

This work opens the possibility to model humps behavior without the previously imposed restrictions on the interconnecting resistance, which not necessarily must be the geometrical value. These results show how with this degree of freedom, the obtained diodes, at least in this case, present ideality factors of 2 and can be explained by the simple SRH theory.

## Acknowledgements

This work has been supported by the MINECO/FEDER within the framework of the projects Ref. TEC2011-28423-C03 and ENE2014-56069-CA-1-R.

## References

Abbott, M., Cousins, P., Chen, F., Cotter, J., 2005. Laser-induced defects in crystalline silicon solar cells. In: Proceedings of the 31st IEEE PVSC, pp. 1241–1244.

Altermatt, P.P., Heiser, G., Green, M.A., 1996. Numerical quantification and minimization of perimeter losses in high-efficiency silicon solar cells. Prog. Photovoltaics Res. Appl. 4, 355–367.

Ashburn, P., Morgan, D.V., Howes, M.J., 1975. A theoretical and experimental study of recombination in silicon p-n junctions. Solid-State Electron. 18, 569–577.

Breitenstein, O., Altermatt, P.P., Ramspeck, K., Green, M.A., Zhao, J., Schenk, A., 2006. Interpretation of commonly observed I-V characteristics of C-Si cells having ideality factor larger than two. In: Proceedings on the 4th WC on PEC IEEE, pp. 879–884.

Cereceda, E., Barredo-Egusquiza, J., Gutiérrez, J.R., Jimeno, J.C., Fraile, A., Hermanns, L., 2012. Damage reduction of the laser drilling process on back contact solar cells by chemical treatment. In: Proceedings of the 27th EU PVSEC, pp. 832–835.

Du, Z.R., Palina, N., Chen, J., Lin, F., Hong, M.H., Hoex, B., 2012. Impact of KOH etching on laser damage removal and contact formation for Al local back surface field silicon wafer solar cells. In: Proceedings of the 27th EU PVSEC, pp. 1230–1233.

Grohe, A., Harmel, C., Knorz, A., Glunz, S.W., Preu, R., Willeke, G.P., 2006. Selective ablation of anti-reflection coatings for novel metallization techniques. In: Proceedings of the 32nd IEEE PVSC, pp. 1399–1402.

Guo, J.H., Cotter, E., McIntosh, K.R., Fisher, K., Chen, F.W., Karpour, A., 2007. Edge passivation for small-area, high efficiency solar cells. In: Proceedings of the 22nd EU PVSEC, pp. 1348–1351.

Gutscher, S., Knorz, A., Gundel, P., Greulich, J., Preu, R., 2008. Characterization and optimization of laser edge isolation. In: Proceedings of the 25th EU PVSEC, pp. 2287–2291.

Hernando, F., Gutiérrez, J.R., Bueno, G., Recart, F., Rodríguez, V., 1998. Humps, a surface damage explanation. In: Proceedings of the 2nd WCPEC, pp. 1321–1323.

Kühn, R., Fath, P., Bucher, E., 2000. Effects of pn-junctions bordering on surfaces investigated by means of 2D-modeling. In: Proceedings of the 28th IEEE PVSC, pp. 116–119.

Kyeong, D., Gunasekarn, M., Kim, K., Kim, H., Kwon, T., Moon, I., Kim, Y., Han, K., 2009. Laser edge isolation for high-efficiency crystalline solar cells. J. Korean Phys. Soc. 55, 124–128.

Martínez, V., Lizundia, R., Jimeno, J.C., 1992. MultIV a Computer Program to Fit I-V Characteristics. In: Proceedings of the 11th EU PVSEC, pp. 314–317.

McIntosh, K.R., Honsberg, C.B., 2001. The influence of edge recombination on a solar cell's I-V curve. In: Proceedings of the 17th EU PVSEC, pp. 1578–1581.

McIntosh, K.R., Altermatt, P.P., Heiser, G.A., 2001. Depletion region recombination. When does mDR = 2? Proceedings of the 17th EU PVSEC, pp. 1651–1654.

Otaegi, A., Jimeno, J.C., Salin, F., Saby, J., 2010. Evaluation of different wavelengths fiber-lasers for isolation of the p-n junction of crystalline silicon solar cells. In: Proceedings of the 25th EU PVSEC, pp. 2329–2332.

Otaegi, A., Jimeno, J.C., Salin, F., Saby, J., 2012. New concepts for laser technologies applied to MWT silicon solar cells. In: Proceedings of the 27th EU PVSEC, pp. 2035–2038.

Otaegi, A., Fano, V., Rasool, M.A., Gutiérrez, J.R., Jimeno, J.C., Cereceda, E., 2015. Laser induced damage for crystalline silicon solar cells. In: Proceedings of the 42nd IEEE PVSEC; 978-1-4799-7944-8/15.

Steingrube, S., Breitenstein, O., Ramspeck, K., Glunz, S., Schenk, A., Altermatt, P.P., 2010. Explanation of commonly observed shunt currents in c-Si solar cells by means of recombination statistics beyond Shockle-Read-Hall approximation. J. Appl. Phys. 110, 014515.

Sugianto, A., Tjahjono, B.S., Guo, J.H., Wenham, S.R., 2007. Impact of laser induced defects on the performance of the solar cells using localized laser doped regions beneath the metal contacts. In: Proceedings of the 22nd EU PVSEC, pp. 1759–1762.

Sugianto, A., Bovatsek, J., Wenham, S.R., Tjahjono, B., Xu, G., Yao, Y., Hallam, B., Bai, X., Kuepper, N., Chong, C.M., Patel, R., 2010. 18.5% Laser-doped solar cell on CZ p-type silicon. In: Proceedings of the 37th IEEE PVSEC, pp. 689–694.

Tjahjono, B.S., Guo, J.H., Hameiri, Z., Mai, L., Sugianto, A., Wang, S., Wenham, S.R., 2007. High efficiency solar cell structures through the use of laser doping. In: Proceedings of the 22nd EU PVSEC, pp. 966–969.